

Optimizing superconductivity: from cuprates via nickelates to palladates

Motoharu Kitatani^{a,b}, Liang Si^{c,d}, Paul Worm^d, Jan M. Tomczak^d, Ryotaro Arita^{b,e} and Karsten Held^d

^aDepartment of Material Science, University of Hyogo, Ako, Hyogo 678-1297, Japan

^bRIKEN Center for Emergent Matter Sciences (CEMS), Wako, Saitama, 351-0198, Japan

^cSchool of Physics, Northwest University, Xi'an 710127, China

^dInstitute of Solid State Physics, TU Wien, 1040 Vienna, Austria and

^eResearch Center for Advanced Science and Technology, University of Tokyo 4-6-1, Komaba, Meguro-ku, Tokyo 153-8904, Japan

(Dated: July 29, 2022)

Motivated by cuprate and nickelate superconductors, we perform a comprehensive study of the superconducting instability in the single-band Hubbard model. We calculate the spectrum and superconducting transition temperature T_c as a function of filling and Coulomb interaction for a range of hopping parameters, combining first principles calculations with the dynamical vertex approximation. We find the sweet spot for high T_c to be at intermediate coupling, moderate Fermi surface warping, and low hole doping. Neither nickelates nor cuprates are close to this optimum. Instead, we identify some palladates, notably $\text{RbSr}_2\text{PdO}_3$ and $A'_2\text{PdO}_2\text{Cl}_2$ ($A'=\text{Ba}_{0.5}\text{La}_{0.5}$), to be virtually optimal, while others, such as NdPdO_2 , are too weakly correlated.

Introduction—Ever since the discovery of cuprate superconductivity [1], the material dependence of the transition temperature T_c and exploring routes toward optimizing T_c are a central quest of condensed matter physics. Theoretically, the minimal model for cuprates [2, 3] and nickelates [4, 5] arguably is an effective one-band Hubbard model. Tight-binding parameters can be obtained from *ab initio* calculations, and the relation between model parameters and the experimental T_c has been analyzed [6–18]. However, in the material-specific context a comprehensive study of the model, and how its interaction and hopping parameter influence the predicted T_c , has not been performed systematically due to the difficulty of studying superconductivity reliably in the presence of strong electronic correlations.

The recently discovered nickelate superconductors provide a new perspective to this quest. Similar to cuprates, superconductivity in nickelates emerges from a doped $3d^{9-\delta}$ ($\delta \sim 0.2$) electronic configuration of the transition metal. Besides the initial infinite-layer superconductor $\text{Nd}_{1-x}\text{Sr}_x\text{NiO}_2$ [19–25], substituting neodymium with another lanthanoid [26–28] and also the quintuple-layer compound [29] show superconductivity. This indicates that, akin to cuprates, there is a whole family of nickelate superconductors.

While multi-orbital effects in nickelates are discussed [30–39], recent studies suggest that the single-band picture works well [4, 5, 40, 41] — at least as a first-step approximation and when including the self-doping from the so-called A -pocket. A very recent magnetotransport experiment evidences strong similarities to cuprates and the validity of the single-band $d_{x^2-y^2}$ picture [42]. Together, nickelates and cuprates suggest that a hole-doped d^9 electronic configuration on a square lattice with a predominant $d_{x^2-y^2}$ orbital at the Fermi energy is a common thread of such high- T_c superconductors. Then, naturally, other transition metal oxides with this disposition

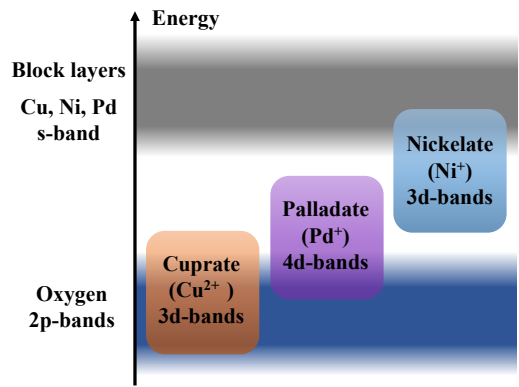


FIG. 1. (Color online) Schematic picture of the energy levels for copper (Cu^{2+}), nickel (Ni^+), palladium (Pd^+) superconductors.

have come into the focus recently, in particular palladates [4, 43–45].

This poses the question: What are the optimal conditions for superconductivity in these cuprate-analog transition metal oxides? One important factor is the interaction strength U and its ratio to the hopping U/t . On a qualitative level it has been recently found [4, 14] that the interaction strength would be too large in nickelates, preventing higher T_c 's and suggesting pressure or compressive strain to enhance T_c [46]. This has already been confirmed experimentally by a record-high $T_c > 30$ K for nickelates under a pressure of 12 GPa with no saturation yet discernible [47], and also significantly higher T_c on a $(\text{La},\text{Sr})(\text{Al},\text{Ta})\text{O}_3$ (LSAT) instead of a SrTiO_3 substrate [48], which induces a compressive strain. Theoretically, it is expected that U/t decreases much more dramatically when going from $3d$ to $4d$ transition metal oxides, which can be achieved by replacing Ni with Pd.

Let us sketch the electronic structures of the above-mentioned materials schematically in Fig. 1. As is well

known, the parent cuprate compounds are charge transfer insulators [49]; Cu-3d and O-2p bands exist at a similar energy level and are strongly hybridized. Thus the Hubbard model is justified only as an effective model that mimics the physics of the Zhang-Rice singlet [3]. In contrast, the Ni 3d-orbital is higher up in energy by ~ 1 eV. The increased distance to the oxygen orbitals then makes the single- $d_{x^2-y^2}$ -orbital description more suitable than for the CuO₂ layers in cuprates. However, density-functional theory (DFT) calculations [30, 45, 50–56] show that the Ni-*d* bands of NdNiO₂ now partially overlap with the bands of Nd in-between the NiO₂ layers, forming pockets around the *A* and — depending on the rare earth atom and concentration of doped hole [57–59] — the Γ momentum. If we replace Ni (3d) with Pd (4d), the Pd 4d-orbitals are shifted back down by ~ 1 eV, since the larger core charge attracts electrons more strongly and the larger band-width in Pd-4d leads to a stronger *d*-*p* orbital mixing. Indeed, our DFT computations (shown in Supplementary Materials (SM) [60] Section I-II) of the crystal and electronic structures of the nickelate NdNiO₂ and the palladates NdPdO₂, RbSr₂PdO₃ and A'_2 PdO₂Cl₂ show that palladate compounds are somewhere in-between cuprates and nickelates — with a single-band $d_{x^2-y^2}$ Fermi surface topology. Tuning the dispersion and interaction strength in palladates opens so-far untapped possibilities for finding new superconductors with possibly higher T_c 's.

In this Letter, we perform a comprehensive study on superconductivity in the single-band Hubbard model, with the objective to harness this possibility. Beyond the filling- and interaction-dependence of the one-particle spectrum, recent progress in diagrammatic techniques allows us to analyze material trends in magnetic and superconducting fluctuations: We find that the optimal condition for a large T_c is intermediate coupling with a sizable next (third) nearest hoping and low hole doping. Combining dynamical vertex approximation (DGA) with first principle calculations, we conclude that some palladates possess the potential for a particularly high T_c .

Model and Method—We study the two-dimensional Hubbard model on the square lattice with Hamiltonian

$$\mathcal{H} = \sum_{\mathbf{k},\sigma} \epsilon_{\mathbf{k}} c_{\mathbf{k},\sigma}^\dagger c_{\mathbf{k},\sigma} + U \sum_i n_{i,\uparrow} n_{i,\downarrow}, \quad (1)$$

where $c_{\mathbf{k},\sigma}^\dagger (c_{\mathbf{k},\sigma})$ is the creation (annihilation) operator,

$$\epsilon_{\mathbf{k}} = -2t[\cos(k_x) + \cos(k_y)] - 4t'\cos(k_x)\cos(k_y) - 2t''[\cos(2k_x) + \cos(2k_y)], \quad (2)$$

the energy-momentum dispersion, U the onsite Coulomb repulsion, and t, t', t'' are the nearest, second nearest, and third nearest hoppings, respectively. The model parameters are obtained from density-functional theory (DFT), using WIEN2K [61] with the PBE [62] exchange corre-

	$ t (\text{meV})$	t'/t	t''/t	U_{eff}/t
NdNiO ₂	395	-0.25	0.12	8
NdNiO ₂ (Strained)	419	-0.23	0.12	7.0–7.5
NdPdO ₂	558	-0.17	0.13	4.5
RbSr ₂ PdO ₃	495	-0.24	0.16	6
A'_2 PdO ₂ Cl ₂	443	-0.22	0.14	7.5
A'_2 PdO ₂ Cl ₂ (-1.5% strain)	470	-0.22	0.14	7.0
A'_2 PdO ₂ Cl ₂ (-3.0% strain)	497	-0.22	0.14	6.0

TABLE I. Summary of the DFT-derived parameters for the single-band Hubbard model, as an effective low-energy model for the nickelate NdNiO₂, the palladates NdPdO₂, RbSr₂PdO₃, and A'_2 PdO₂Cl₂.

lation functional and WIEN2WANNIER [63] for projecting onto a maximally localized $3d_{x^2-y^2}$ Wannier orbital [64]. When constructing the single-orbital model for palladates, we performed multi-orbital DMFT calculations and confirmed the single orbital nature of the system, see SM [60] for details. The constrained random phase approximation (cRPA) is employed to estimate U . Following the previous research [4], we employed slightly enhanced values (+0.35 eV [65]) from our cRPA calculation for entangled bands [66]: 2.85 eV for NdNiO₂, 2.55 eV for RbSr₂PdO₂, and 2.97 eV for A'_2 PdO₂Cl₂ (which are consistent with the preceding study [45]; please note that the small change of the interaction strength U does not change our conclusion). Table I provides a summary of the DFT and cRPA derived parameters (for details see SM [60] Section II), which are used in subsequent DGA calculations. Besides these material-specific Hubbard models we also include the simplest case with nearest-neighbor hopping only ($t' = t'' = 0$).

We analyze these single-orbital models by means of the dynamical vertex approximation (DGA) [67–70], a diagrammatic extension of dynamical mean-field theory (DMFT) [71–73]. Similar techniques have been previously applied to unconventional superconductivity on the square lattice [74–81]. We mainly use the continuous-time quantum Monte-Carlo solver from w2dynamics [82] as DMFT solver, see SM [60] for details. DGA simultaneously includes strong correlations and long-range spatial (charge and spin) fluctuations. Both are essential for modelling superconductivity in correlated electron systems. Most importantly, DGA can describe the dynamical screening effect which are crucial for accurately determining T_c [83]. It has predicted the superconducting dome in nickelates [4] prior to experiments [21, 48, 84] with astonishing accuracy. For a review of DGA, see [85]; and [86] for how to calculate T_c .

Spectrum—We first discuss the electronic spectrum. In Fig. 2, we show the momentum dependence of the imaginary part of the Green's function at the lowest Matsubara frequency: $-\Im G(\omega_n = \pi/\beta, \mathbf{k})/\pi$ for $U/t = 4.3, 6, 7, 8$, $n = 0.80, 0.85, 0.90, 0.95$ for hoppings corre-

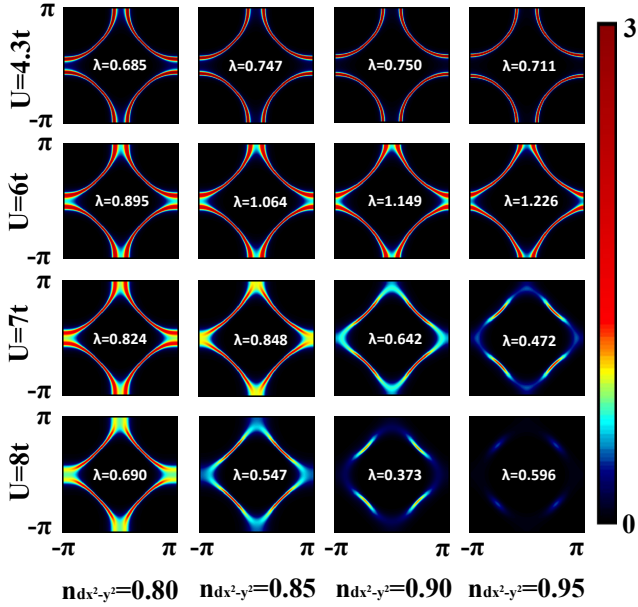


FIG. 2. (Color online) DGA Spectrum (momentum dependence of the imaginary part of the Green function $-\Im G/\pi$ at lowest Matsubara frequency) for different interactions ($U/t = 4.3, 6.0, 7.0, 8.0$) and fillings ($n = 0.80, 0.85, 0.90, 0.95$) at $T = 0.01t$, $t'/t = -0.17$, $t''/t = 0.13$. Corresponding d -wave superconductivity eigenvalues λ are also shown.

sponding to NdPdO₂ ($t'/t = -0.17$, $t''/t = 0.13$). We observe that the spectrum changes from a non-interacting-like Fermi surface at weak coupling to a shape with strongly momentum-dependent damping at stronger coupling, before, finally, all spectral weight is removed. In between, we obtained a Fermi arc structure at low doping ($n_{d_{x^2-y^2}} \sim 0.90 - 0.95$) for $U = 7t$ and $8t$, which is a hallmark feature of cuprates.

Even outside the pseudogap region, correlation effects change the Fermi surface structure. Specifically, they decrease the Fermi surface warping, i.e. effectively decrease t' . Such change of the spectrum for large (t', t'') region has also been observed in other theoretical studies [87–89]. These Fermi surface changes also effect the superconducting instability. While this effect (coming from the momentum dependence of $\Re \Sigma$) is minor compared with the pseudogap physics (stemming from the momentum dependence of $\Im \Sigma$), we find that such a Fermi surface flattening can enhance superconductivity, but only around the optimal conditions in parameter space; see SM [60] for a detailed discussion.

As demonstrated here, DGA properly captures correlation induced changes of the Fermi surface (e.g., Fermi arc in cuprates [90]) and is consistent with previous results. *Superconductivity*—Next, we discuss the superconducting instability. To do so, we calculate the eigenvalues of the linearized gap (Eliashberg) equation which is the

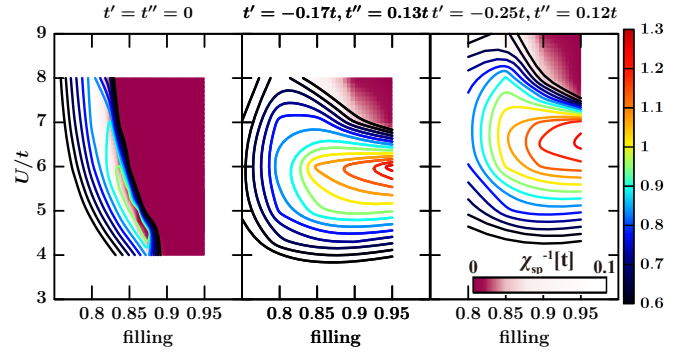


FIG. 3. (Color online) Superconducting eigenvalue λ and antiferromagnetic susceptibility $\chi_{sp}(Q_{\max}, \omega = 0)$ as a function of interaction U and filling at $T = 0.01t$ for the three different t', t'' given at the top of each panel.

usual procedure for evaluating the superconducting instability from the paramagnetic solution. The eigenvalue λ is a measure of the superconducting instability, and T_c is identified by λ reaching unity. While DGA is unbiased with respect to spin, charge and quantum critical fluctuations, we find that spin fluctuations mediate d -wave superconductivity in all cases studied.

In Fig. 3, we plot the superconducting eigenvalues against the interaction U and the filling for three tight-binding parameter sets: the simplest case ($t' = t'' = 0$), parameters for NdPdO₂ ($t' = -0.17t$, $t'' = 0.13t$) and NdNiO₂ ($t' = -0.25t$, $t'' = 0.12t$). First, we notice in all cases a strong suppression of λ around half-filling at strong coupling. This leads to a dome structure of T_c as a function of both interaction strength and filling, which is essential for optimizing superconducting materials.

Fig. 3 unequivocally reveals that the origin of this suppression are too strong antiferromagnetic correlations (dark red color scale). These open a pseudogap in Fig. 2 and thus suppress the electron propagator. Even though the antiferromagnetic pairing glue is huge, this eventually suppresses superconductivity.

Let us note that cluster DMFT [91] shows a similar tendency as in Fig. 3, albeit with still much higher temperatures and weaker superconducting fluctuations. The pseudogap behavior is, on the other hand, consistent with the observation that the insulating regime expands if long-range spatial fluctuations are properly included [92–94].

Except for the perfectly nested case ($t' = t'' = 0$) where spin-fluctuation are overly strong and open a gap regardless of interaction strength, we can separate the U -range into two regions: For weak couplings ($U \lesssim 5$), there is only a weak doping dependence. For strong coupling ($U \gtrsim 7$), on the other hand, a pronounced filling dependence develops, with antiferromagnetic fluctuation dominating around half-filling and suppressing λ . Optimal conditions for superconductivity in the one-band 2D square-lattice Hubbard model are realized in between

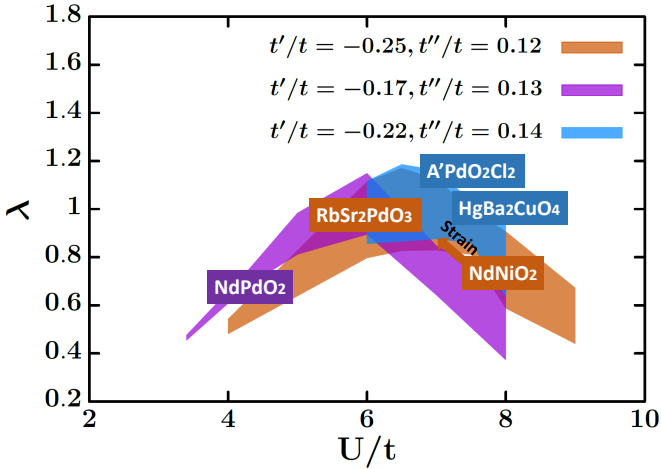


FIG. 4. (Color online) Interaction U dependence of the superconducting eigenvalues λ at $T = 0.01t$ for three different t', t'' from Table I. For each U , the linewidth corresponds to the range of λ for fillings $0.80 \leq n \leq 0.90$. Materials corresponding to these models and U 's are indicated.

these two regions. The importance of the finite Fermi surface warping was also suggested in early phenomenological material-dependence studies of cuprate superconductors [6]. The only other possibilities to significantly enhance T_c are (i) increasing t , which sets the energy scale, while keeping all parameter ratios constant, or (ii) creating a positive feedback on superconductivity from other bands including the oxygen bands in case of cuprates.

Fig. 4 demonstrates that a dome shape of λ develops as a function of U . The optimal U slightly depends on the (t', t'') parameters. This trend can be explained by the earlier onset of the pseudogap for systems with small t', t'' , due to better (antiferromagnetic) nesting.

In Fig. 4, we also show the points corresponding to each material from Table I. Further we include $\text{HgBa}_2\text{CuO}_4$ as a typical cuprate which has $U/t \sim 7.5t - 8t$ [13, 15, 16] and almost the same t', t'' as $\text{A}'_2\text{PdO}_2\text{Cl}_2$. As mentioned in previous works [4, 14], we can see that NdNiO_2 has a too large interaction and thus falls outside the area with highest T_c .

Following this insight, we can rationalize now the recent experimental achievements of realizing higher T_c 's in NdNiO_2 : both external pressure [47] and in-plane lattice compressive strains [48, 95] play similar roles at reducing the in-plane lattice constant, shrinking the Ni-Ni distance and weakening the correlation strength U/t , while increasing the magnetic exchange $4t^2/U$ [96]. Simply replacing Ni-3d by Pd-4d yields NdPdO_2 which is too weakly correlated in Fig. 4. A promising solution to increase U/t is to enlarge the lattice which is possible by inserting spacing layers between the PdO_2 planes. Doing so, our DFT and cRPA calculations indeed place $\text{RbSr}_2\text{PdO}_3$ and $\text{A}'_2\text{PdO}_2\text{Cl}_2$ close to the optimum.

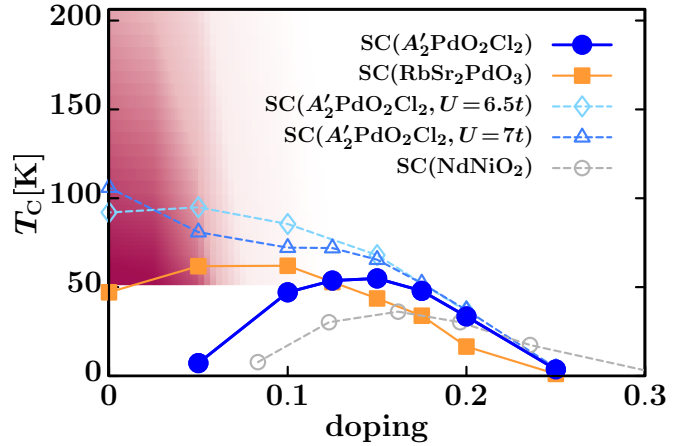


FIG. 5. (Color online) Phase diagrams for nickelates (NdNiO_2) and palladates ($\text{RbSr}_2\text{PdO}_3$ and $\text{A}'_2\text{PdO}_2\text{Cl}_2$). In the red region, we expect antiferromagnetism instead of superconductivity for $\text{A}'_2\text{PdO}_2\text{Cl}_2$ if there is a weak inter-layer coupling because of the huge χ_{sp} (color code as in Fig. 3).

We finally show in Fig. 5 the phase diagram for these palladate compounds, using the same approach as previously for nickelates [4]. We predict palladates to have a $T_c \gtrsim 60$ K, which touches the floor level line of cuprates and remarkably exceeds the current upper limit of nickelates, $T_c = 30$ K [47, 48]. Indeed, the calculated phase diagram (superconductivity and antiferromagnetism) for $\text{A}'_2\text{PdO}_2\text{Cl}_2$ is quite similar to well-known cuprate phase diagrams. Furthermore, weak strain (described by $U = 6.5t, 7t$ [97], c.f., Table I) would tune the material to an even higher T_c .

Conclusion and outlook—Building on the success of DGA to predict the superconducting dome in nickelates, we have performed a comprehensive survey of the Hubbard model and revealed the optimal phase-space region for unconventional superconductivity. The optimal condition is at intermediate coupling ($U/t = 6 - 7$), moderate Fermi surface warping ($|t'| + |t''| \approx 0.3 - 0.4$), and low hole doping ($n \sim 0.90 - 0.95$). Combining this insight with first principles calculations, we predict palladates and nickelates grown on compressive substrates to be superconductors with a T_c comparable to cuprates.

The theoretically proposed palladates have yet to be synthesized. Palladates with a perovskite-like structure [98, 99], however, have already been realized in experiment. Then, provided that a reduction process, similar to that of $\text{NdNiO}_3 \rightarrow \text{NdNiO}_2$, is possible, realizing palladates with PdO_2 layers is a promising route for high- T_c superconductors. Additionally, the possibility to engineer cuprate analogs based on 4d materials has been discussed based on AgF_2 [100] and silver oxides [101]. Analyzing the relation between those systems and the ones we are proposing in this letter will offer fresh insight into the design of superconductors.

Acknowledgments—We would like to thank Motoaki Hirayama and Yusuke Nomura for illuminating discussions. We acknowledge the financial support by Grants-in-Aids for Scientific Research (JSPS KAKENHI) Grant No. JP21K13887 and JP19H05825 as well as by project P32044 of the Austrian Science Funds (FWF). Calculations have been done mainly on the Vienna Scientific Cluster (VSC).

[1] J. G. Bednorz and K. A. Müller, *Zeitschrift für Physik B Condensed Matter* **64**, 189 (1986).

[2] P. W. Anderson, *Science* **235**, 1196 (1987).

[3] F. C. Zhang and T. M. Rice, *Phys. Rev. B* **37**, 3759 (1988).

[4] M. Kitatani, L. Si, O. Janson, R. Arita, Z. Zhong, and K. Held, *npj Quantum Materials* **5**, 59 (2020).

[5] J. Karp, A. S. Botana, M. R. Norman, H. Park, M. Zingl, and A. Millis, *Phys. Rev. X* **10**, 021061 (2020).

[6] E. Pavarini, I. Dasgupta, T. Saha-Dasgupta, O. Jepsen, and O. K. Andersen, *Phys. Rev. Lett.* **87**, 047003 (2001).

[7] H. Sakakibara, H. Usui, K. Kuroki, R. Arita, and H. Aoki, *Phys. Rev. Lett.* **105**, 057003 (2010).

[8] C. Weber, C. Yee, K. Haule, and G. Kotliar, *EPL (Europhysics Letters)* **100**, 37001 (2012).

[9] H. Sakakibara, K. Suzuki, H. Usui, S. Miyao, I. Maruyama, K. Kusakabe, R. Arita, H. Aoki, and K. Kuroki, *Phys. Rev. B* **89**, 224505 (2014).

[10] S. W. Jang, H. Sakakibara, H. Kino, T. Kotani, K. Kuroki, and M. J. Han, *Scientific reports* **6**, 1 (2016).

[11] S. Teranishi, K. Nishiguchi, and K. Kusakabe, *Journal of the Physical Society of Japan* **87**, 114701 (2018).

[12] M. Hirayama, Y. Yamaji, T. Misawa, and M. Imada, *Phys. Rev. B* **98**, 134501 (2018).

[13] F. Nilsson, K. Karlsson, and F. Aryasetiawan, *Phys. Rev. B* **99**, 075135 (2019).

[14] H. Sakakibara and T. Kotani, *Phys. Rev. B* **99**, 195141 (2019).

[15] M. Hirayama, T. Misawa, T. Ohgoe, Y. Yamaji, and M. Imada, *Phys. Rev. B* **99**, 245155 (2019).

[16] S. Teranishi, K. Nishiguchi, and K. Kusakabe, *Journal of the Physical Society of Japan* **90**, 054705 (2021).

[17] H. Watanabe, T. Shirakawa, K. Seki, H. Sakakibara, T. Kotani, H. Ikeda, and S. Yunoki, *Phys. Rev. Research* **3**, 033157 (2021).

[18] J.-B. Morée, M. Hirayama, M. T. Schmid, Y. Yamaji, and M. Imada, arXiv preprint arXiv:2206.01510 (2022).

[19] D. Li, K. Lee, B. Y. Wang, M. Osada, S. Crossley, H. R. Lee, Y. Cui, Y. Hikita, and H. Y. Hwang, *Nature* **572**, 624 (2019).

[20] L. Si, W. Xiao, J. Kaufmann, J. M. Tomczak, Y. Lu, Z. Zhong, and K. Held, *Phys. Rev. Lett.* **124**, 166402 (2020).

[21] S. Zeng, C. S. Tang, X. Yin, C. Li, M. Li, Z. Huang, J. Hu, W. Liu, G. J. Omar, H. Jani, Z. S. Lim, K. Han, D. Wan, P. Yang, S. J. Pennycook, A. T. S. Wee, and A. Ariando, *Phys. Rev. Lett.* **125**, 147003 (2020).

[22] D. Li, B. Y. Wang, K. Lee, S. P. Harvey, M. Osada, B. H. Goodge, L. F. Kourkoutis, and H. Y. Hwang, *Phys. Rev. Lett.* **125**, 027001 (2020).

[23] M. Hepting, D. Li, C. J. Jia, H. Lu, E. Paris, Y. Tseng, X. Feng, M. Osada, E. Been, Y. Hikita, and et al., *Nature Materials* (2020), 10.1038/s41563-019-0585-z.

[24] Y. Nomura and R. Arita, *Reports on Progress in Physics* **85**, 052501 (2022).

[25] J. Karp, A. Hampel, and A. J. Millis, *Phys. Rev. B* **105**, 205131 (2022).

[26] M. Osada, B. Y. Wang, K. Lee, D. Li, and H. Y. Hwang, *Phys. Rev. Materials* **4**, 121801 (2020).

[27] S. Zeng, C. Li, L. E. Chow, Y. Cao, Z. Zhang, C. S. Tang, X. Yin, Z. S. Lim, J. Hu, P. Yang, and A. Ariando, *Science Advances* **8**, eabl9927 (2022).

[28] M. Osada, B. Y. Wang, B. H. Goodge, S. P. Harvey, K. Lee, D. Li, L. F. Kourkoutis, and H. Y. Hwang, *Advanced Materials* **33**, 2104083 (2021).

[29] G. A. Pan, D. F. Segedin, H. LaBollita, Q. Song, E. M. Nica, B. H. Goodge, A. T. Pierce, S. Doyle, S. Novakov, D. C. Carrizales, A. T. N'Diaye, P. Shafer, H. Paik, J. T. Heron, J. A. Mason, A. Yacoby, L. F. Kourkoutis, O. Erten, C. M. Brooks, A. S. Botana, and J. A. Mundy, *Nature Materials* (2021), 10.1038/s41563-021-01142-9.

[30] P. Werner and S. Hoshino, *Phys. Rev. B* **101**, 041104 (2020).

[31] F. Lechermann, *Phys. Rev. B* **101**, 081110 (2020).

[32] F. Lechermann, *Phys. Rev. X* **10**, 041002 (2020).

[33] F. Petocchi, V. Christiansson, F. Nilsson, F. Aryasetiawan, and P. Werner, *Phys. Rev. X* **10**, 041047 (2020).

[34] P. Adhikary, S. Bandyopadhyay, T. Das, I. Dasgupta, and T. Saha-Dasgupta, *Phys. Rev. B* **102**, 100501 (2020).

[35] Y. Wang, C.-J. Kang, H. Miao, and G. Kotliar, *Phys. Rev. B* **102**, 161118 (2020).

[36] Z. Wang, G.-M. Zhang, Y.-f. Yang, and F.-C. Zhang, *Phys. Rev. B* **102**, 220501 (2020).

[37] E. Been, W.-S. Lee, H. Y. Hwang, Y. Cui, J. Zaanen, T. Devreux, B. Moritz, and C. Jia, *Phys. Rev. X* **11**, 011050 (2021).

[38] X. Wan, V. Ivanov, G. Resta, I. Leonov, and S. Y. Savrasov, *Phys. Rev. B* **103**, 075123 (2021).

[39] T. Y. Xie, Z. Liu, C. Cao, Z. F. Wang, J. L. Yang, and W. Zhu, *Phys. Rev. B* **106**, 035111 (2022).

[40] K. Higashi, M. Winder, J. Kuneš, and A. Hariki, *Phys. Rev. X* **11**, 041009 (2021).

[41] P. Worm, L. Si, M. Kitatani, R. Arita, J. M. Tomczak, and K. Held, arXiv preprint arXiv:2111.12697 (2021).

[42] W. Sun, Y. Li, R. Liu, J. Yang, J. Li, S. Yan, H. Sun, W. Guo, Z. Gu, Y. Deng, et al., arXiv preprint arXiv:2204.13264 (2022).

[43] A. S. Botana and M. R. Norman, *Phys. Rev. Materials* **2**, 104803 (2018).

[44] K. Held, L. Si, P. Worm, O. Janson, R. Arita, Z. Zhong, J. M. Tomczak, and M. Kitatani, *Frontiers in Physics* **9** (2022), 10.3389/fphy.2021.810394.

[45] M. Hirayama, T. Tadano, Y. Nomura, and R. Arita, *Phys. Rev. B* **101**, 075107 (2020).

[46] L. Si, P. Worm, and K. Held, *Crystals* **12** (2022), 10.3390/cryst12050656.

[47] N. N. Wang, M. W. Yang, K. Y. Chen, Z. Yang, H. Zhang, Z. H. Zhu, Y. Uwatoko, X. L. Dong, K. J. Jin, J. P. Sun, and J. G. Cheng, arXiv:2109.12811 (2021).

[48] K. Lee, B. Y. Wang, M. Osada, B. H. Goodge, T. C. Wang, Y. Lee, S. Harvey, W. J. Kim, Y. Yu, C. Murthy, S. Raghu, L. F. Kourkoutis, and H. Y. Hwang,

arXiv:2203.02580 (2022).

[49] J. Zaanen, G. A. Sawatzky, and J. W. Allen, *Phys. Rev. Lett.* **55**, 418 (1985).

[50] A. S. Botana and M. R. Norman, *Phys. Rev. X* **10**, 011024 (2020).

[51] H. Sakakibara, H. Usui, K. Suzuki, T. Kotani, H. Aoki, and K. Kuroki, *Phys. Rev. Lett.* **125**, 077003 (2020).

[52] L.-H. Hu and C. Wu, *Phys. Rev. Research* **1**, 032046 (2019).

[53] X. Wu, D. Di Sante, T. Schwemmer, W. Hanke, H. Y. Hwang, S. Raghu, and R. Thomale, *Phys. Rev. B* **101**, 060504 (2020).

[54] Y. Nomura, M. Hirayama, T. Tadano, Y. Yoshimoto, K. Nakamura, and R. Arita, *Phys. Rev. B* **100**, 205138 (2019).

[55] G.-M. Zhang, Y.-f. Yang, and F.-C. Zhang, *Phys. Rev. B* **101**, 020501 (2020).

[56] M. Jiang, M. Berciu, and G. A. Sawatzky, *Phys. Rev. Lett.* **124**, 207004 (2020).

[57] L. Si, J. Kaufmann, Z. Zhong, J. M. Tomeczak, and K. Held, *Phys. Rev. B* **104**, L041112 (2021).

[58] I. Leonov, S. L. Skornyakov, and S. Y. Savrasov, *Phys. Rev. B* **101**, 241108 (2020).

[59] S. Ryee, H. Yoon, T. J. Kim, M. Y. Jeong, and M. J. Han, *Phys. Rev. B* **101**, 064513 (2020).

[60] Supplemental information regarding details of DFT, DMFT and DGA calculations, as well as spectra, are available at XXX.

[61] P. Blaha, K. Schwarz, F. Tran, R. Laskowski, G. K. H. Madsen, and L. D. Marks, *The Journal of Chemical Physics* **152**, 074101 (2020).

[62] J. P. Perdew, K. Burke, and M. Ernzerhof, *Phys. Rev. Lett.* **77**, 3865 (1996).

[63] J. Kuneš, R. Arita, P. Wissgott, A. Toschi, H. Ikeda, and K. Held, *Computer Physics Communications* **181**, 1888 (2010).

[64] N. Marzari, A. A. Mostofi, J. R. Yates, I. Souza, and D. Vanderbilt, *Rev. Mod. Phys.* **84**, 1419 (2012).

[65] We employed a slightly different version of crRPA calculations [66] than previously [4], to better capture material differences. While we still enhance U to mimic the frequency dependence and other over-screening effects, the enhancement used here is slightly smaller than in Ref. 4.

[66] T. Miyake, F. Aryasetiawan, and M. Imada, *Phys. Rev. B* **80**, 155134 (2009).

[67] A. Toschi, A. A. Katanin, and K. Held, *Phys. Rev. B* **75**, 045118 (2007).

[68] K. Held, A. Katanin, and A. Toschi, *Progress of Theoretical Physics (Supplement)* **176**, 117 (2008).

[69] A. A. Katanin, A. Toschi, and K. Held, *Phys. Rev. B* **80**, 075104 (2009).

[70] H. Kusunose, *J. Phys. Soc. Jpn.* **75**, 054713 (2006).

[71] W. Metzner and D. Vollhardt, *Phys. Rev. Lett.* **62**, 324 (1989).

[72] A. Georges, G. Kotliar, W. Krauth, and M. J. Rozenberg, *Rev. Mod. Phys.* **68**, 13 (1996).

[73] G. Kotliar and D. Vollhardt, *Physics Today* **57**, 53 (2004).

[74] J. Otsuki, H. Hafermann, and A. I. Lichtenstein, *Phys. Rev. B* **90**, 235132 (2014).

[75] M. Kitatani, N. Tsuji, and H. Aoki, *Phys. Rev. B* **92**, 085104 (2015).

[76] M. Kitatani, N. Tsuji, and H. Aoki, *Phys. Rev. B* **95**, 075109 (2017).

[77] J. Vučičević, T. Ayral, and O. Parcollet, *Phys. Rev. B* **96**, 104504 (2017).

[78] D. Vilardi, C. Taranto, and W. Metzner, *Phys. Rev. B* **99**, 104501 (2019).

[79] S. Sayyad, E. W. Huang, M. Kitatani, M.-S. Vaezi, Z. Nussinov, A. Vaezi, and H. Aoki, *Phys. Rev. B* **101**, 014501 (2020).

[80] G. V. Astretsov, G. Rohringer, and A. N. Rubtsov, *Phys. Rev. B* **101**, 075109 (2020).

[81] M. Kitatani, Y. Nomura, M. Hirayama, and R. Arita, arXiv preprint arXiv:2205.00239 (2022), 10.48550/arXiv.2205.00239.

[82] M. Wallerberger, A. Hausoel, P. Gunacker, A. Kowalski, N. Parragh, F. Goth, K. Held, and G. Sangiovanni, *Computer Physics Communications* **235**, 388 (2019).

[83] M. Kitatani, T. Schäfer, H. Aoki, and K. Held, *Phys. Rev. B* **99**, 041115 (2019).

[84] D. Li, B. Y. Wang, K. Lee, S. P. Harvey, M. Osada, B. H. Goodge, L. F. Kourkoutis, and H. Y. Hwang, *Phys. Rev. Lett.* **125**, 027001 (2020).

[85] G. Rohringer, H. Hafermann, A. Toschi, A. A. Katanin, A. E. Antipov, M. I. Katsnelson, A. I. Lichtenstein, A. N. Rubtsov, and K. Held, *Rev. Mod. Phys.* **90**, 025003 (2018).

[86] M. Kitatani, R. Arita, T. Schäfer, and K. Held, *Journal of Physics: Materials* **5**, 034005 (2022).

[87] W. Wu, M. S. Scheurer, S. Chatterjee, S. Sachdev, A. Georges, and M. Ferrero, *Phys. Rev. X* **8**, 021048 (2018).

[88] R. Rossi, F. Šimkovic, and M. Ferrero, *EPL (Europhysics Letters)* **132**, 11001 (2020).

[89] M. Klett, P. Hansmann, and T. Schäfer, *Frontiers in Physics* **10** (2022), 10.3389/fphy.2022.834682.

[90] T. Yoshida, X. J. Zhou, K. Tanaka, W. L. Yang, Z. Hussain, Z.-X. Shen, A. Fujimori, S. Sahrakorpi, M. Lindroos, R. S. Markiewicz, A. Bansil, S. Komiya, Y. Ando, H. Eisaki, T. Kakeshita, and S. Uchida, *Phys. Rev. B* **74**, 224510 (2006).

[91] X. Chen, J. P. F. LeBlanc, and E. Gull, *Phys. Rev. Lett.* **115**, 116402 (2015).

[92] T. Schäfer, F. Geles, D. Rost, G. Rohringer, E. Arrigoni, K. Held, N. Blümer, M. Aichhorn, and A. Toschi, *Phys. Rev. B* **91**, 125109 (2015).

[93] F. Šimkovic, J. P. F. LeBlanc, A. J. Kim, Y. Deng, N. V. Prokof'ev, B. V. Svistunov, and E. Kozik, *Phys. Rev. Lett.* **124**, 017003 (2020).

[94] T. Schäfer, N. Wentzell, F. Šimkovic, Y.-Y. He, C. Hille, M. Klett, C. J. Eckhardt, B. Arzhang, V. Harkov, F. m. c.-M. Le Régent, A. Kirsch, Y. Wang, A. J. Kim, E. Kozik, E. A. Stepanov, A. Kauch, S. Andergassen, P. Hansmann, D. Rohe, Y. M. Vilk, J. P. F. LeBlanc, S. Zhang, A.-M. S. Tremblay, M. Ferrero, O. Parcollet, and A. Georges, *Phys. Rev. X* **11**, 011058 (2021).

[95] X. Ren, Q. Gao, Y. Zhao, H. Luo, X. Zhou, and Z. Zhu, arXiv preprint arXiv:2109.05761 (2021), 10.48550/arXiv.2109.05761.

[96] O. Ivashko, M. Horio, W. Wan, N. B. Christensen, D. E. McNally, E. Paris, Y. Tseng, N. E. Shaik, H. M. Rønnow, H. I. Wei, C. Adamo, C. Lichtensteiger, M. Gibert, M. R. Beasley, K. M. Shen, J. M. Tomczak, T. Schmitt, and J. Chang, *Nature Communications* **10**, 786 (2019).

[97] For drawing the $U = 6.5t$ phase diagram, we averaged

the -1.5% , -3.0% -strain result from Table I.

- [98] S.-J. Kim, S. Lemaux, G. Demazeau, J.-Y. Kim, and J.-H. Choy, *Journal of Materials Chemistry* **12**, 995 (2002).
- [99] S.-J. Kim, S. Lemaux, G. Demazeau, J.-Y. Kim, and J.-H. Choy, *Journal of the American Chemical Society* **123**, 10413 (2001).
- [100] J. Gawraczyński, D. Kurzydłowski, R. A. Ewings, S. Bandaru, W. Gadomski, Z. Mazej, G. Ruani, I. Bergenti, T. Jaroń, A. Ozarowski, *et al.*, *Proceedings of the National Academy of Sciences* **116**, 1495 (2019).
- [101] M. Hirayama, M. Thobias Schmid, T. Tadano, T. Misawa, and M. Imada, [arXiv:2207.12595](https://arxiv.org/abs/2207.12595) (2022).

Supplementary material for "Optimizing superconductivity: from cuprates via nickelates to palladates"

Motoharu Kitatani^{a,b}, Liang Si^{c,d}, Paul Worm^d, Jan M. Tomczak^d, Ryotaro Arita^{b,e} and Karsten Held^d

^aDepartment of Material Science, University of Hyogo, Ako, Hyogo 678-1297, Japan

^bRIKEN Center for Emergent Matter Sciences (CEMS), Wako, Saitama, 351-0198, Japan

^cSchool of Physics, Northwest University, Xi'an 710127, China

^dInstitute of Solid State Physics, TU Wien, 1040 Vienna, Austria and

^eResearch Center for Advanced Science and Technology, University of Tokyo 4-6-1, Komaba, Meguro-ku, Tokyo 153-8904, Japan

(Dated: July 29, 2022)

This supplementary material contains additional results obtained by density functional theory (DFT), dynamical mean field theory (DMFT) and dynamical vertex approximation (DFA) that further corroborate our conclusions of the main text and is organized in five sections. In Section I, we perform discussions on the crystal structures, parameters and analyze similarities and differences between the nickelate NdNiO_2 and the palladates NdPdO_2 , $\text{RbSr}_2\text{PdO}_3$ and $\text{A}'_2\text{PdO}_2\text{Cl}_2$ ($\text{A}' = \text{La}_{0.5}\text{Ba}_{0.5}$). Section II provides detailed DFT (and beyond DFT) results of electronic structure computations for all compounds. In Section III we show the DMFT results, including spectral functions and effective mass, for $\text{RbSr}_2\text{PdO}_3$ and $\text{A}'_2\text{PdO}_2\text{Cl}_2$. Section IV shows the self-energy effect on the spectrum and the superconductivity instability in more detail. Finally, in Section V, we show the numerical details on the DFA study of superconductivity.

I. CRYSTAL STRUCTURE OF NICKELATES AND PALLADATES

The crystal structures of nickelate NdNiO_2 and palladates NdPdO_2 , $\text{RbSr}_2\text{PdO}_3$ and $\text{A}'_2\text{PdO}_2\text{Cl}_2$ are shown in Fig. S.1. To guarantee a $3d^9$ configuration of the Ni^{1+} cation in $\text{A}'_2\text{PdO}_2\text{Cl}_2$, we need a $\text{A}'^{2.5+}$ cation which can be achieved by mixing 50%La and 50%Ba. To approach optimal filling/doping in the proposed palladates $\text{RbSr}_2\text{PdO}_3$ and $\text{A}'_2\text{PdO}_2\text{Cl}_2$, the ration between $\text{Rb}^{1+}/\text{Sr}^{2+}$ for the former and $\text{La}^{3+}/\text{Ba}^{2+}$ for the later case can be tuned.

The relaxed parameters for all nickelates and palladates are shown in Table S.I. For the DFT-level calculations, PBESol [1] is employed for structural relaxations, and PBE [2] for electronic structure calculations (e.g., DFT band structures and tight-binding Wannier projections), following the lines of Ref. [3]. Our PBESol structural relaxations yield the lattice constants of NdNiO_2 $a=b=3.864 \text{ \AA}$ and $c=3.243 \text{ \AA}$. To simulate in-plane compressive strain effects, we tune the in-plane lattices to 3.800 \AA [of bulk LaAlO_3 (LAO)], the z -lattice is then simultaneously relaxed to 3.330 \AA . assuming that the films are several layers thick as in experiments for nickelate superconductors, this change of the lattice parameters is the dominant effect of the substrate; apart from that a bulk DFT calculation is justified. The corresponding changes of hoppings and U are shown in Table I of the main text.

For NdPdO_2 , an in-plane lattice expansion from 3.864 \AA to 4.085 \AA results from substituting Ni by Pd. Such an expansion may contribute to smaller orbital overlap and stronger electronic correlations if the B -site atoms are unchanged, however the more delocalized $4d$ -

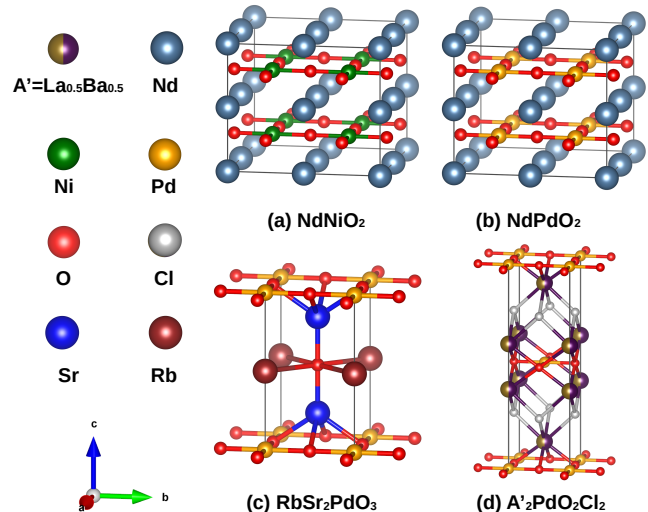


FIG. S.1. Crystal structures of (a) NdNiO_2 , (b) NdPdO_2 , (c) $\text{RbSr}_2\text{PdO}_3$ and (d) $\text{A}'_2\text{PdO}_2\text{Cl}_2$.

orbitals of Pd counteract this with their larger orbital spreads (see main text). When the in-plane lattices are fixed to the one of SrTiO_3 to simulate the strain effects from a STO substrate, the out-of-plane is relaxed to 3.255 \AA , which boosts its two-dimensional characters.

For the proposed palladates $\text{RbSr}_2\text{PdO}_3$ and $\text{A}'_2\text{PdO}_2\text{Cl}_2$, the in-plane lattice constants are even larger than those of NdPdO_2 . Another notable difference is the distance between Ni-Ni or Pd-Pd along the z -direction (out-of-plane); it increases to $\sim 7.5\text{--}8.0 \text{ \AA}$, as shown in Table S.I. In the last column we list some suitable substrates for the proposed materials, e.g., for $\text{RbSr}_2\text{PdO}_3$ and strained (-1.5% and 3%)

TABLE S.I. DFT-PBESol relaxed lattice parameters of NdNiO_2 , NdPdO_2 (with full relaxation or grown on SrTiO_3 substrate), $\text{RbSr}_2\text{PdO}_3$ and $A'_2\text{PdO}_2\text{Cl}_2$ (in units of Å). A' is $\text{La}_{0.5}\text{Ba}_{0.5}$. In the last column we show the appropriate substrates, in the brackets are the in-plane lattice constants (also in unit of Å).

-	a/b	c	Ni-Ni/Pd-Pd (in-plane)	out-of-plane	Substrate
NdNiO_2	3.864	3.243	3.864	3.243	LSAT (3.868)
NdNiO_2 (strained: on LaAlO_3)	3.800	3.330	3.800	3.330	LaAlO_3 (3.80)
NdPdO_2	4.085	3.143	4.085	3.143	PrScO_3 (4.02)
NdPdO_2 (strained: on SrTiO_3)	3.905	3.255	3.905	3.255	SrTiO_3 (3.905)
$\text{RbSr}_2\text{PdO}_3$	4.264	7.555	4.264	7.555	MgO (4.20)
$A'_2\text{PdO}_2\text{Cl}_2$ (unstrained)	4.366	14.639	4.366	7.944	Rutile- TiO_2 (4.59)/ MgO (4.20)
$A'_2\text{PdO}_2\text{Cl}_2$ (-1.5% strain)	4.301	14.740	4.301	7.973	MgO (4.20)
$A'_2\text{PdO}_2\text{Cl}_2$ (-3% strain)	4.235	14.870	4.235	8.016	MgO (4.20)

$A'_2\text{PdO}_2\text{Cl}_2$ that host larger in-plane lattice constants than SrTiO_3 (3.905 Å), MgO is considerable to be employed as substrate as its in-plane lattice is ~ 4.2 Å. For the fully relaxed NdPdO_2 (4.085 Å), PrScO_3 (in-plane lattice 4.02 Å) is possible candidate. For compressive cases (when compared with the in-plane lattice of SrTiO_3 : 3.905 Å) such as unstrained NdNiO_2 and strained NdNiO_2 , one of the possible substrates (LaAlO_3)_{0.3}($\text{SrAl}_{0.5}\text{Ta}_{0.5}\text{O}_3$)_{0.7} (LSAT: 3.868 Å) had been proved as helpful to enhance its T_c [4]. For the strained case, LaAlO_3 (3.80 Å) is expected to be more effective at eliminating atomic defects and enhancing T_c . The in-plane lattice constant of unstrained $A'_2\text{PdO}_2\text{Cl}_2$ is predicted as 4.366 Å in DFT structural relaxation, we hence proposed rutile- TiO_2 (4.59 Å) and MgO (4.20 Å) as a possible substrate in realistic experiments.

II. ELECTRONIC STRUCTURE OF NICKELATES AND PALLADATES

To investigate the difference between nickelates and palladates, we first compute their band centroids. The bands centroids in Table S.II are computed by $E_i = \int g_i(E)EdE / \int g_i(E)$, here g_i is the partial density of states of the corresponding orbital i and E is the energy. The integration ranges covers both the bonding and anti-bonding states for Cu/Ni/Pd- d orbital and O- p orbitals (up to 5, 7 and 7 eV for CaCuO_2 , NdNiO_2 and NdPdO_2 , respectively). As one can see, for the cuprate CaCuO_2 , both the centroids of Cu- d and $d_{x^2-y^2}$ are just ~ 0.4 eV and ~ 0.7 eV higher than that of O- p . This is consistent with the fact that CaCuO_2 is a charge-transfer insulator.

For NdNiO_2 , the d -bands ($d_{x^2-y^2}$ band) shift up by ~ 1 eV (~ 0.9 eV) compared with those in CaCuO_2 . Moreover, the O- p bands are shifted down by ~ 0.9 eV. As a consequence, the charge transfer energies $\Delta(d-p)$ and $\Delta(d_{x^2-y^2}-p)$ in NdNiO_2 are ~ 1.8 eV larger than in CaCuO_2 .

For the palladate NdPdO_2 , the band centroid of d -

orbitals $E(d)$ is comparable with those of CaCuO_2 while $E(d_{x^2-y^2})$ is ~ 0.3 eV higher than in CaCuO_2 . Thus, the charge transfer energies $\Delta(d-p)$ and $\Delta(d_{x^2-y^2}-p)$ are 1.211 and 1.827 eV, i.e., in between the charge transfer energies of CaCuO_2 and NdNiO_2 . The computations strongly hint that NdPdO_2 hosts a similar 2D nature as in both CaCuO_2 and NdNiO_2 .

In Fig. S.2 we show the DFT-level band structures of NdPdO_2 and $\text{RbSr}_2\text{PdO}_3$ and $A'_2\text{PdO}_2\text{Cl}_2$. NdPdO_2 has a larger $d_{x^2-y^2}$ bandwidth than NdNiO_2 , which is due to its more delocalized 4 d orbitals nature. Its pockets at Γ and A are energetically deeper than in NdNiO_2 . However, as concluded by previous research [5], these pockets are not essential for emergent nickelate superconductivity. Additionally, the band structures of $A'_2\text{PdO}_2\text{Cl}_2$ [Fig. S.2(d)] exhibits a Fermi structure with only the Pd- $d_{x^2-y^2}$ orbital. For $\text{RbSr}_2\text{PdO}_3$ [Fig. S.2(c)], the pockets merely touch the Fermi energy at the A and Γ momentum. Indeed, the tiny Γ pocket for $\text{RbSr}_2\text{PdO}_3$ is expected to become unoccupied upon hole doping or with exchange-correlations by using functional beyond standard DFT-PBE: the Γ -pocket is absent, e.g., for $\text{Rb}_{1.2}\text{Sr}_{1.8}\text{PdO}_3$ [Fig. S.3(a)] and $\text{RbSr}_2\text{PdO}_3$ computed by employing the improved version of the modified Becke-Johnson (mBJ) exchange potential [Fig. S.3(b)]. On a technical note, the process of hole doping and consequently the noninteger filling at Pd- $d_{x^2-y^2}$ in $\text{RbSr}_2\text{PdO}_3$ is achieved here by employing virtual crystal approximation [6].

In Fig. S.3, the band structures of NdPdO_2 [Fig. S.3(d)] on a SrTiO_3 substrate, $\text{RbSr}_2\text{PdO}_3$ upon 0.2 hole doping per Pb (i.e., $\text{Rb}_{1.2}\text{Sr}_{1.8}\text{PdO}_3$) [Fig. S.3(a)], and the bands calculated by improved version of the modified Becke-Johnson exchange potential [7] [Fig. S.3(b)] are shown; for a comparison further the band of fully relaxed NdPdO_2 are presented in Fig. S.3(c). As shown in Fig. S.3(a-b), both hole doping and exchange-correlation potentials are shift the Γ pocket of $\text{RbSr}_2\text{PdO}_3$ above the Fermi energy E_f . These results demonstrate that the realistic Fermi surface of $\text{RbSr}_2\text{PdO}_3$ can also be expected

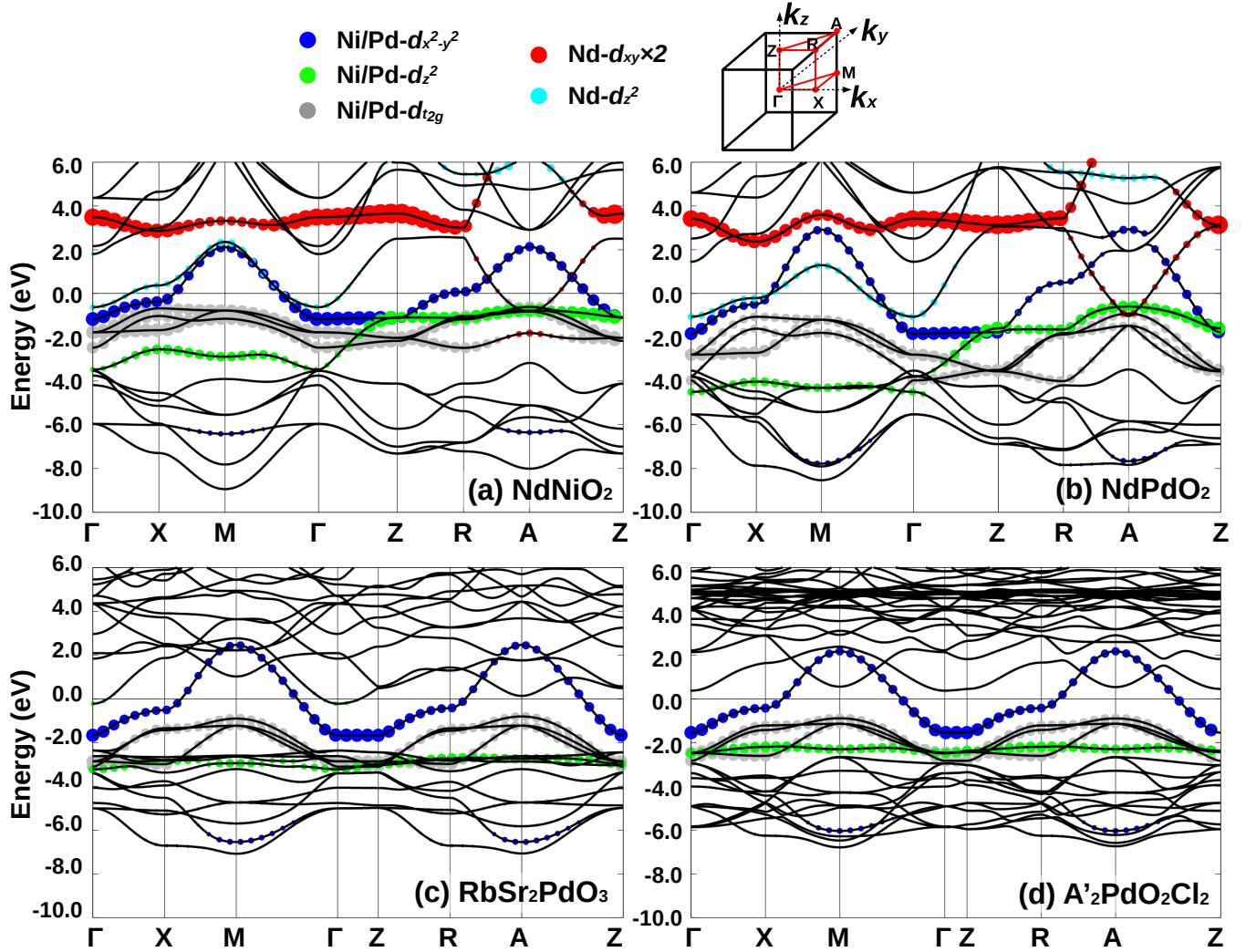


FIG. S.2. DFT band characters of (a) NdNiO_2 , (b) NdPdO_2 , (c) $\text{RbSr}_2\text{PdO}_3$ and (d) $\text{A}'\text{PdO}_2\text{Cl}_2$. Here, we used the fully relaxed structure for all systems. The top panel shows the symbols for different orbitals and the first Brillouin zone. The size of the symbols for $\text{Nd}-d_{xy}$ are renormalized by a factor of 2 for clearness.

to be composed of a single band with $d_{x^2-y^2}$ character, even without additional hole doping. The correlations from Pd-4d and the exchange effects, which are both only rudimentarily accounted for in DFT, play an effective role at preserving a 2D cuprates-like Fermi surface.

As we discussed in the main text, the fully relaxed in-plane lattice constants of NdPdO_2 are $a=b=4.085 \text{ \AA}$, 4.6% more than a SrTiO_3 substrate: 3.905 \AA . A suitable substrate for an almost unstrained film is PrScO_3 whose lattice is 4.02 \AA (as shown in Table S.I). If NdPdO_2 is grown on SrTiO_3 , the in-plane lattice is fixed as 3.905 \AA . As a consequence, the out-of-plane lattice is relaxed to larger value of 3.255 \AA , and thus a better 2D character of the $d_{x^2-y^2}$ orbital. As shown in [Fig. S.3(c-d)], such a strain does not change the main character of the Pd- $d_{x^2-y^2}$ orbital.

Finally, as Pd is heavier than Ni, one may consider

TABLE S.II. DFT calculated band centeroids (in units of eV) of CaCuO_2 , NdNiO_2 and NdPdO_2 and charge transfer energies Δ .

-	$E(d)$	$E(d_{x^2-y^2})$	$E(O-p)$	$\Delta(d-p)$	$\Delta(d_{x^2-y^2}-p)$
CaCuO_2	-2.367	-2.047	-2.772	0.405	0.725
NdNiO_2	-1.384	-1.148	-3.674	2.289	2.525
NdPdO_2	-2.358	-1.742	-3.570	1.211	1.827

the spin-orbital coupling (SOC) effects in palladates. We hence perform DFT+SOC band computations for NdPdO_2 (fully relaxed case) with and without SOC, as shown in Fig. S.4. Fig. S.4(a) and (b) show the DFT band of NdPdO_2 without and with SOC, respectively. For better visibility, we also plot these bands in a smaller energy region from -2 to 4 eV in Fig. S.4 (c,d). We find

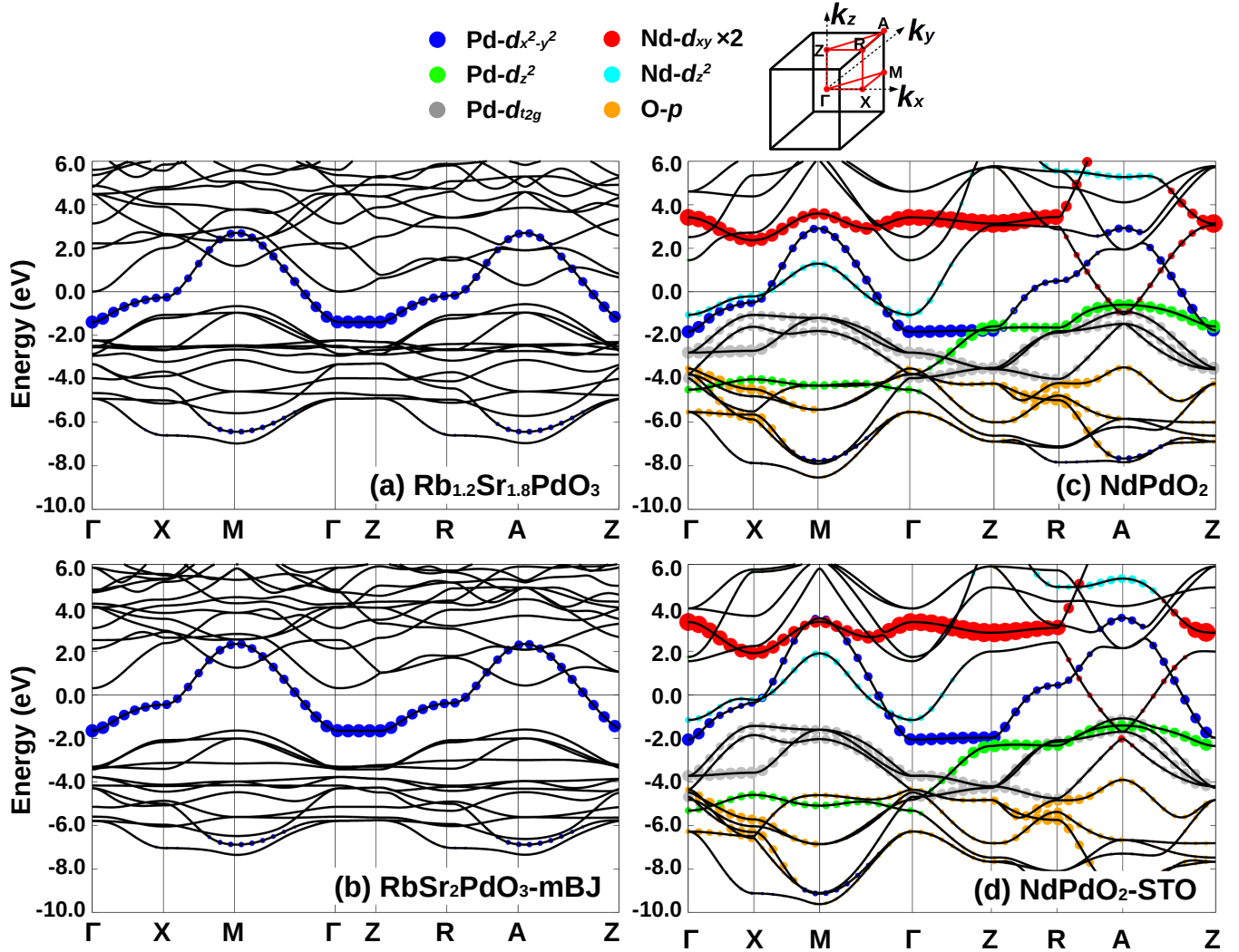


FIG. S.3. Comparison between the DFT band characters of (a) hole doped $\text{Rb}_{1.2}\text{Sr}_{1.8}\text{PdO}_3$, (b) $\text{RbSr}_2\text{PdO}_3$ with mBJ exchange-correlation functional, (c) fully relaxed NdPdO_2 and (d) NdPdO_2 on SrTiO_3 (STO) substrate. The top panel shows the symbols for contribution of the different orbitals and the first Brillouin zone. The size of the symbols for $\text{Nd}-d_{xy}$ are renormalized by a factor of 2 for clearness.

three band-crossing regions in which hybridization gaps open after switching-on SOC effect, see S.4(c). The first region is at $E \sim 1$ to -2 eV and $k=X-M$. Here, the SOC opens a hybridization gap between the $\text{Pd}-t_{2g}$ bands. The second region is at $E \sim 0.5$ eV and $k=A$, where there is a band-crossing between $\text{Nd}-d_{xy}$ orbitals, which mostly contribute to the A -pocket, and $\text{Pd}-t_{2g}$ bands. Since these two regions are irrelevant to our target $\text{Pd}-d_{x^2-y^2}$ band, the effect on superconductivity will be minor. The third region is at $E \sim 2$ eV and $k=A$. In Fig. S.4(c), as one see that there is a double-band degeneracy composed of $\text{Nd}-d_{yz}$ and d_{xz} bands, labeled by the arrow in (c). This double degeneracy exchanges its band characters with $\text{Pd}-d_{x^2-y^2}$ band at A -point. And the gap opens after including SOC effect because the double degeneracy between $\text{Nd}-d_{yz}$ and $\text{Nd}-d_{xz}$ is lost, as shown in the

orange region in Fig. S.4(d). However, we can exclude this small band-opening as a possible factor suppressing superconductivity in palladates because the energy of this gap is high (~ 2 eV) compared to E_f at the very top of the energy region of $\text{Pd}-d_{x^2-y^2}$ band (-2 to 3 eV). Additionally, hole-doping will further reduce E_f and weaken this hybridization.

All in all, we conclude that for the low energy physics around the Fermi level, the SOC does not play an important role. This is because there is only a single $\text{Pd}-d_{x^2-y^2}$ band crossing the Fermi level. While SOC could be disadvantageous for superconductivity, in principle, for superconductivity in the studied palladates it does not seem to be relevant. Hence, we do not consider it in the subsequent DMFT and DGA calculations.

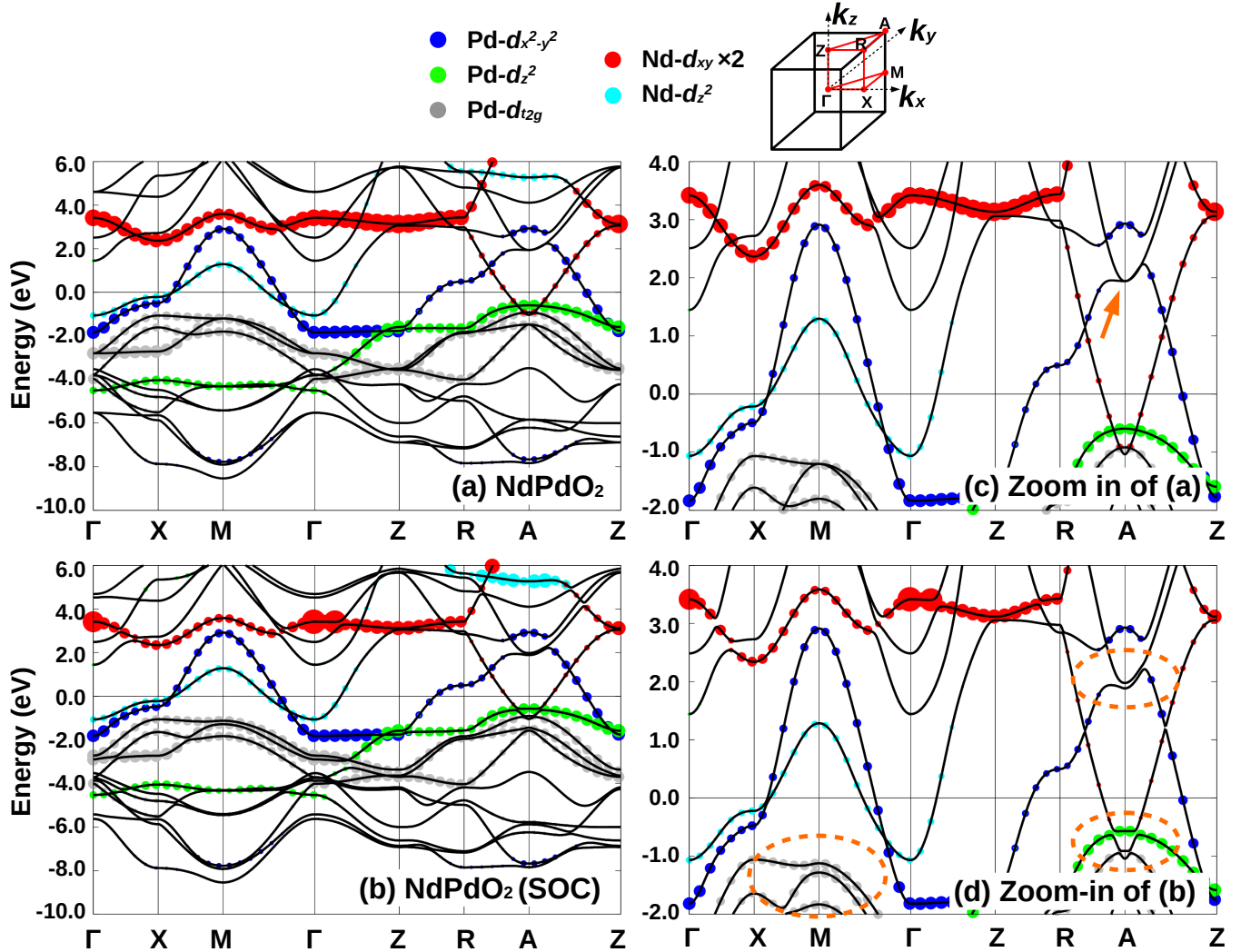


FIG. S.4. Comparison between the DFT band characters of NdPdO₂ with (a,c) and without (b,d) SOC. The arrow in (c) indicates the double degeneracy of the Nd- d_{yz} and Nd- d_{xz} orbital at the A point. The dashed orange regions in (d) indicate the SOC induced hybridization gaps.

III. FULL *d*-SHELL PROJECTION IN DMFT

The DFT bands are projected onto maximumly localized Wannier functions [8–11] of (i) only the Pd $d_{x^2-y^2}$ band (for the single-band DMFT and DGA calculations presented in the main text) and of (ii) all Pd *d* bands (for the full-*d* set calculations in this section), using the WANNIER90 [12] and WIEN2WANNIER [13] codes. These corresponding low-energy effective tight-binding Hamiltonians are generated and subsequently supplemented by a local Kanamori interaction, using the fully localized limit as double counting [14]. DMFT calculations in the present research are carried out at 300 K with the W2DYNAMICS code [15], which solves the corresponding impurity problem using the continuous time quantum Monte Carlo (CTQMC) approach in the hybridization expansion (CT-HYB) [16]. Real-frequency spectra are

obtained with the ANA_CONT code [17] via analytic continuation using the maximum entropy method (MaxEnt) [18, 19].

The corresponding DMFT results of R_dSr₂PdO₃ and A'₂PdO₂Cl₂ are shown in Fig. S.5, Fig. S.6 and Fig. S.7. Fig. S.5 shows the DMFT *k*-resolved ($A(k, \omega)$) and *k*-integrated spectral function ($A(\omega)$) spectral functions of the parent compounds R_dSr₂PdO₃ [Fig. S.5(a)] and A'₂PdO₂Cl₂ [Fig. S.5(b)], i.e., at 4*d*⁹ Pd electronic configuration which corresponds to a half-filled Pd- $d_{x^2-y^2}$ orbital. Including DMFT electronic correlations, the other *d*-bands ($t_{2g}+d_{z^2}$) of Pd are well separated from the $d_{x^2-y^2}$ band. This makes both R_dSr₂PdO₃ and A'₂PdO₂Cl₂ electronically similar to cuprates superconductors.

Large hole doping had been proved being able to destroy the single-band picture and suppress superconduc-

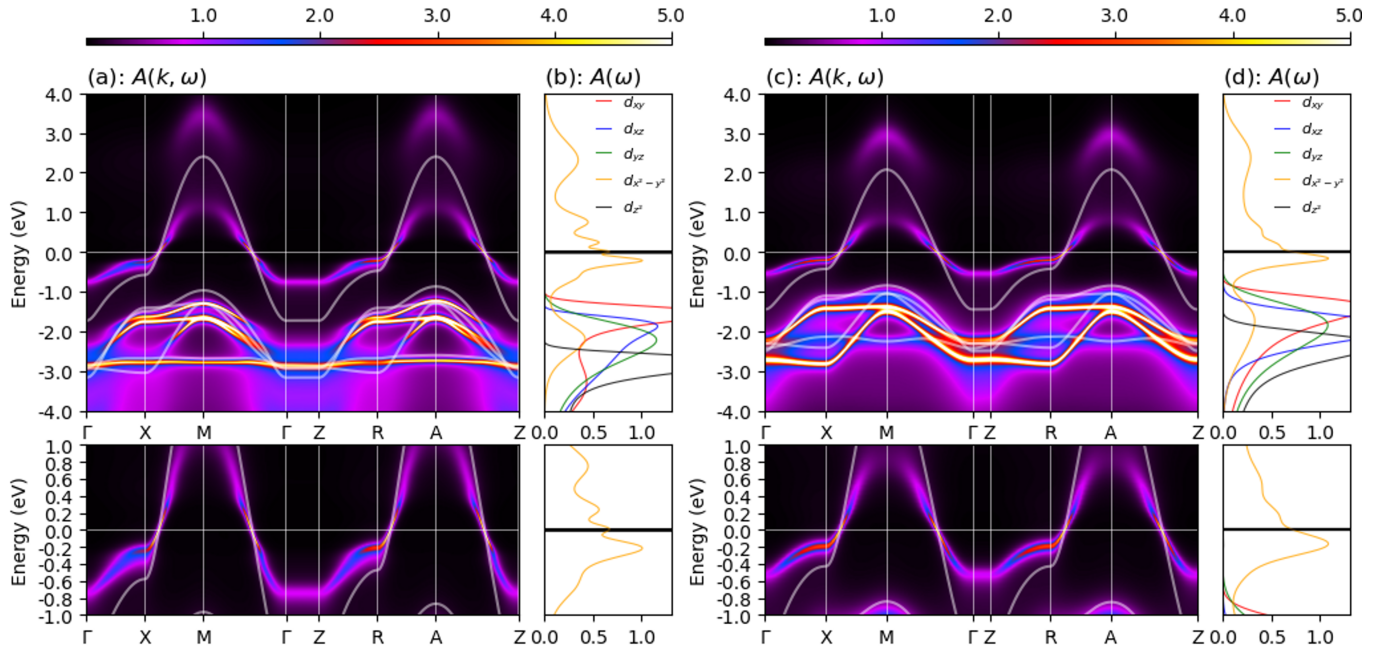


FIG. S.5. Spectral function, k -resolved ($A(k, \omega)$) and k -integrated ($A(\omega)$), for a full d -shell projection at a nominal filling of $n = 9.0$. (Left) $\text{RdSr}_2\text{PdO}_3$ and (right) $\text{A}'_2\text{PdO}_2\text{Cl}_2$.

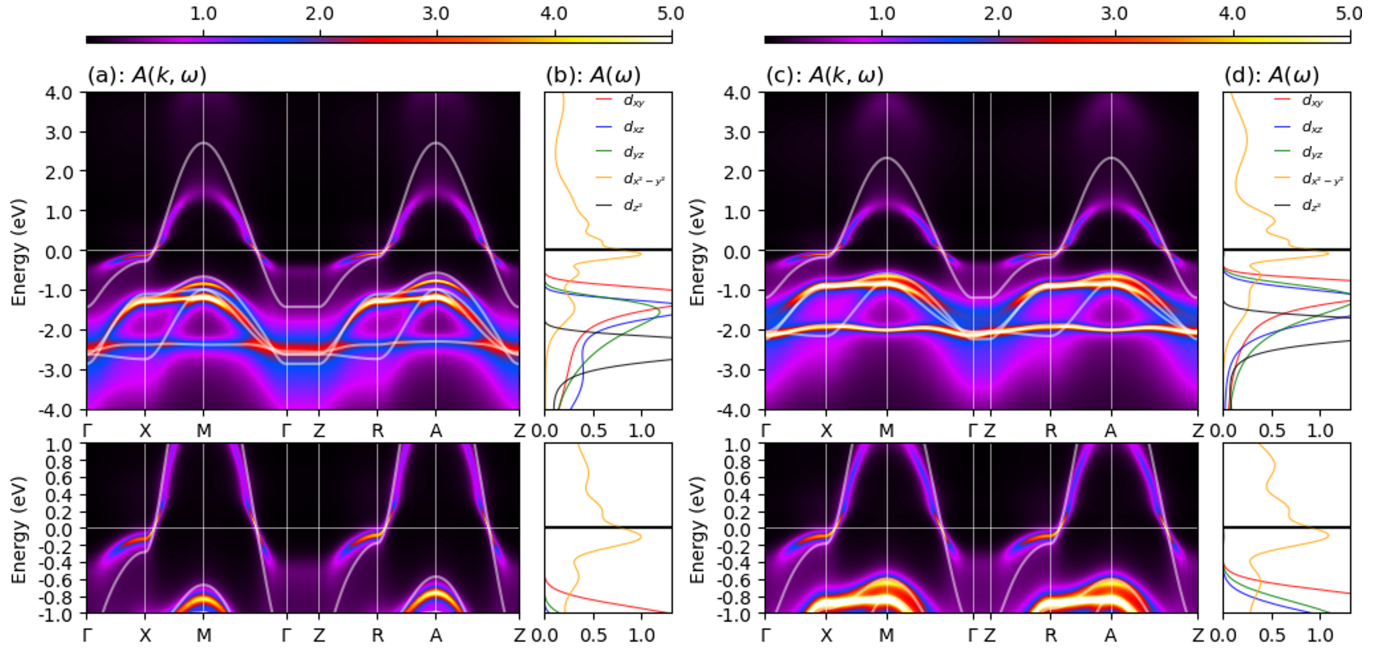


FIG. S.6. Same as Fig. S.5 but now at a nominal filling of $n = 8.8$, which corresponds to the superconducting region.

tivity states in both cuprates and nickelates. Hence it is worth to investigate the electronic structures of $\text{RdSr}_2\text{PdO}_3$ and $\text{A}'_2\text{PdO}_2\text{Cl}_2$ with a certain amount of hole doping, in particular, in the hole doping region were superconductivity may be expected. Here, we show the DMFT spectra of $\text{Rd}_{1.2}\text{Sr}_{1.8}\text{PdO}_3$ ($4d^{8.8}$) and

$\text{A}'_2\text{PdO}_2\text{Cl}_2$ (with $\text{A}'^{2.4+} = (\text{La}_{0.4}\text{Ba}_{0.6})^{2.4+}$ and consequently $4d^{8.8}$). For both compounds, the single-band $d_{x^2-y^2}$ Fermi surface is conserved.

Finally, we investigate the effective mass (m^*) of both compounds. Fig. S.7 displays the mass renormalization of the $d_{x^2-y^2}$ band as obtained in DMFT (including

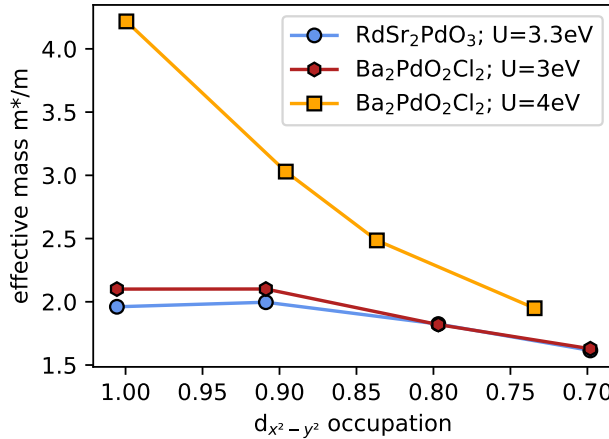


FIG. S.7. Effective mass (m^*/m) as a function of $d_{x^2-y^2}$ occupation for $RdSr_2PdO_3$ at $U = 3.3\text{eV}$ (blue) and $Ba_2PdO_2Cl_2$ at $U = 3\text{eV}$ (red) and $U = 4\text{eV}$ (orange).

all Pd d orbitals). For the $A'_2PdO_2Cl_2$ compound we show two values of the interaction strength: $U=3.3\text{eV}$ for $RdSr_2PdO_3$, 3.3eV and 4eV for $A'_2PdO_2Cl_2$. As antiferromagnetic correlations become large towards half-filling so does the effective mass, in particular for the larger interaction. This indicates the strong tendency toward an anti-ferromagnetic Mott insulator at strong coupling. The mass renormalization for both $RdSr_2PdO_3$ and $A'_2PdO_2Cl_2$ at optimal filling for superconductivity, i.e. $n \sim 1 - 0.8$, is around $m^*/m \sim 2$, which is consistent with the values of $NdNiO_2$ as n approaches ~ 0.82 per Ni - $d_{x^2-y^2}$: $m^*/m = 2.81$. This comparison indicates that these palladates are quite strongly correlated but less so than $NdNiO_2$. This is advantageous for superconductivity, as discussed in the main text.

IV. EFFECT OF FERMI SURFACE SHAPE ON T_c

As shown in the main text, the self-energy weakens the spectral intensity and flattens the Fermi surface shape. Here, we discuss these effects on the Fermi surface structure in more detail, by artificially separating the different effects.

In Fig. S.8, we show the spectrum at two interaction strength [(a) $U = 7.5t$ and (b) $U = 6.5t$] comparing the full DGA and DMFT self-energy [top left (DGA) and top right subpanels (DMFT) in (a) and (b)] to the following artificially modified DGA self-energies: only the real part [$\text{Im}\Sigma = 0$; middle left subpanels], only the imaginary part [$\text{Re}\Sigma = 0$; bottom left subpanels], momentum averaged DGA self-energy [Σ_{ave} , middle right subpanels] and momentum average for the real part only, keeping the momentum-dependence of the imaginary part [$\text{Re}\Sigma_{\text{ave}}$, bottom right subpanels]. We fix the filling to the origi-

nal value (i.e., recalculate the chemical potential) for all cases. We also show the corresponding superconductivity eigenvalues λ calculated with these spectra, while keeping the pairing vertex the same for solving the linearized gap equation.

We can first see that the imaginary part of the self-energy has the most relevant effect; it leads to the pseudogap physics, as expected: From DGA to $\text{Im}\Sigma = 0$ in Fig. S.8, the shape of the Fermi surface remains the same, but its intensity becomes stronger, in particular in the antinodal region around $(\pi, 0)$. The corresponding superconducting eigenvalues is a factor 6-7 higher. This clearly shows that the pseudogap is counterproductive for superconductivity.

Comparing DGA to $\text{Im}\Sigma = 0$ and the non-interacting Fermi surface (white dots in the top left subpanels) further shows that the flattening of the Fermi surface is still captured for $\text{Im}\Sigma = 0$. That is it is caused by the real part of the DGA self-energy, hence there is also no flattening in the $\text{Re}\Sigma = 0$ Fermi surface.

Next, if we compare the DMFT self-energy and the momentum averaged DGA self-energy, they give similar results. That is, the Fermi surface structure is similar to the non-interacting case (white dots in top left subpanels). Some self-energy damping exists in both cases, but as a matter of course, there is no momentum differentiation and hence no pseudogap. In this case, the superconductivity eigenvalues are in between those for $\text{Im}\Sigma = 0$ and the DGA self-energy.

When ignoring the momentum dependence of the real part of the self-energy, $\text{Re}\Sigma = 0$ and $\text{Re}\Sigma_{\text{ave}}$ give similar results in Fig. S.8. The Fermi surface is the same as in the non-interacting case, but strong damping exists around the anti-nodal $(\pi, 0)$ region (and symmetrically related momenta). This is a consequence of the momentum differentiation of the imaginary part of the DGA self-energy.

When we focus on the effect of the Fermi surface flattening on superconductivity, we can compare the superconducting eigenvalue λ for $\text{Re}\Sigma = 0$ and $\text{Re}\Sigma_{\text{ave}}$ with the original DGA λ . We surprisingly find the flattening of the Fermi surface suppresses superconductivity at $U = 7.5t, t' = -0.22t, t'' = 0.14t, n = 0.85$ but enhances it at $U = 6.5t, t' = -0.25t, t'' = 0.12t, n = 0.95$.

To study this dichotomy further, We analyze the parameter dependence in Fig. S.9. We can see that there is almost no effect of $\text{Re}\Sigma$ in the weak coupling regime. In contrast, at strong coupling, the eigenvalues are almost everywhere suppressed if the flattening of the Fermi surface is properly included in Fig. S.9 (a). This Fermi surface flattening, given by the real part of the DGA self-energy, enhances T_c only around the optimum in the original phase diagram in Fig. S.9(a). That is, for intermediate U and fillings closer to half filling.

This result can be understood as follows: If the strength of the spectrum is similar, i.e., if there is no

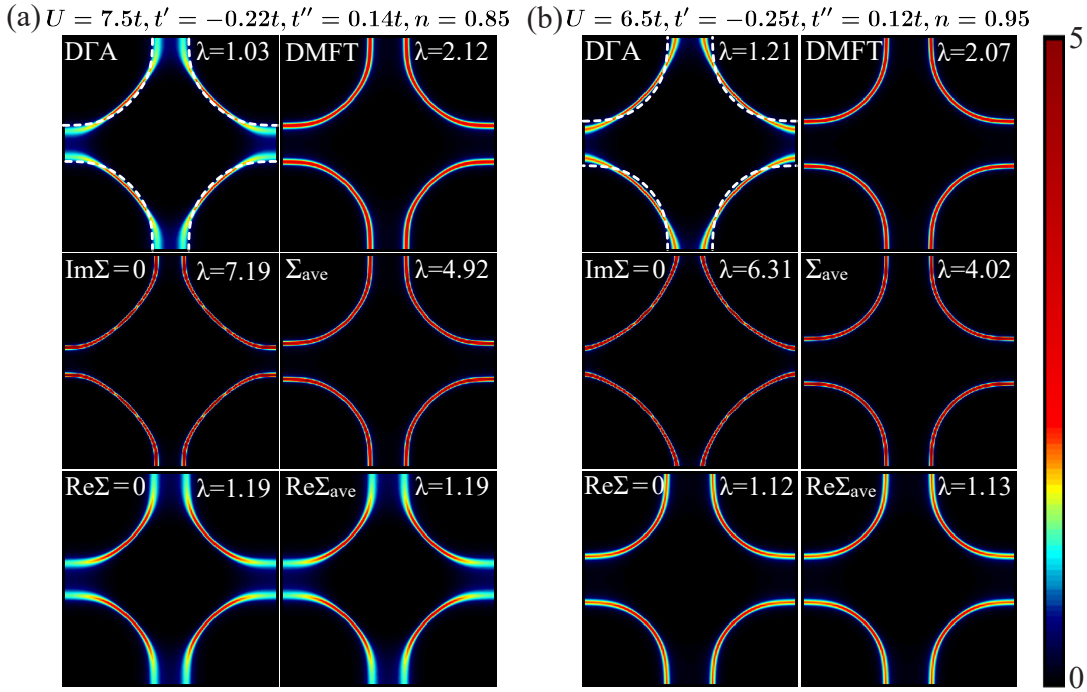


FIG. S.8. Spectrum and superconductivity eigenvalues with DMFT, DGA and artificially modified self-energies (see text) at $\beta t = 100$ for $U = 7.5t$, $t' = -0.22t$, $t'' = 0.14t$, $n = 0.85$ (left) and $U = 6.5t$, $t' = -0.25t$, $t'' = 0.12t$, $n = 0.95$ (right).

pseudogap, spectral weight closer to $(\pi, 0)$ is favorable because the (d -wave) gap function has a peak there and because the van Hove singularity results in a particular strong spectral contribution. On the other hand, if the pseudogap opens around $(\pi, 0)$, this trend will eventually reverse. For weak coupling, the Fermi surface flattening does not occur nor does the pseudogap open. There is hence no effect. For larger interactions, the flattening of the Fermi surface moves the Fermi surface toward $(\pi, 0)$. At intermediate coupling, there is no pseudogap yet [see Fig. S.8 (b)] and superconductivity becomes enhanced. This leads to the optimum (or hot spot) for superconductivity in Fig. S.9 (a) at $U \approx 6t$ and $n \approx 0.95$. In contrast for larger interactions a pseudogap opens [see Fig. S.8 (a)]. Thus despite the flattened Fermi surface, superconductivity is suppressed. If it was possible to switch of this pseudogap [as in the artificial $\text{Im}\Sigma = 0$ panel of Fig. S.8 (a)] we would get the strongest tendency toward superconductivity in this parameter regime.

V. DETAILS OF DGA CALCULATION

In this section, we explain computational details for DGA results. For further details and the general procedure how to calculate spin (and charge) fluctuations and from these superconductivity in (λ -corrected), we refer the reader to [5, 20].

First, for solving the impurity problem and calculating local vertices, which act as a starting point, we use

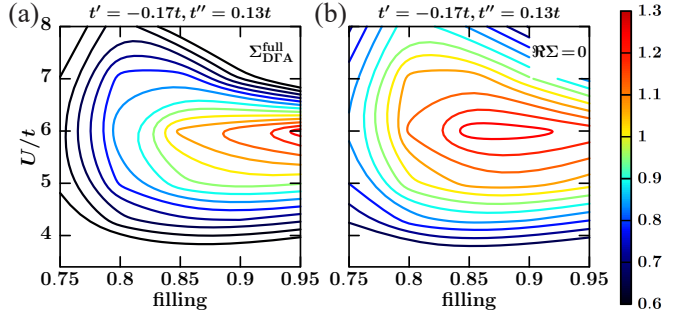


FIG. S.9. Comparison of superconductivity eigenvalues when using the full DGA self-energy ($\Sigma_{\text{DGA}}^{\text{full}}$) and when ignoring the real-part of the self-energy ($\Re\Sigma = 0$), which is responsible for flattening the Fermi surface.

the continuous-time quantum Monte-Carlo (CT-QMC) on w2dynamics [15] as an impurity solver [except for $U = 9t$ results, which are taken from the previous results [5] using exact diagonalization (ED)]. We have also checked that both solvers give quantitatively consistent results at $U = 8t$, $t' = -0.25$, $t'' = 0.12$.

In the DGA calculations, we separate the Matsubara frequency range into two parts following the previous works [5, 20]. We use 120 (80) Matsubara grids for the case $\beta t = 100$, $U \geq 5t$ (others) for which the vertices are treated directly. For an extended grid of 2048 Matsubara frequencies on the positive side we use the bare- U contribution instead of the local vertex. This is sufficient to obtain well-converged results even at low tempera-

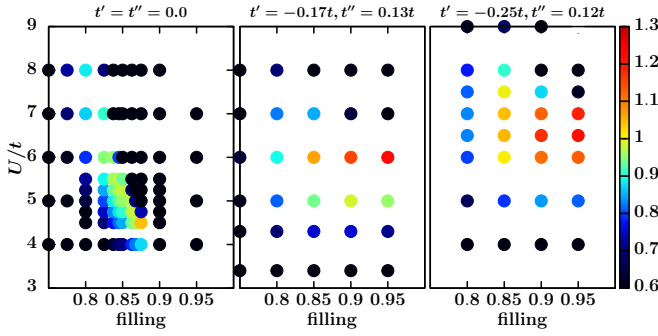


FIG. S.10. Directly calculated points for producing Fig. 3 in the main text. The color corresponds to the superconducting eigenvalue λ at fixed temperature $T = 0.01t$.

tures [21]. For momentum grids, we take a 120×120 momentum mesh, which may not be enough to get quantitatively converged results in the critically fluctuating regime (dark magenta region in Fig. 3), but elsewhere is sufficient [22]. Nevertheless, this mesh is enough to study the superconductivity dominating region, which is the main scope of this paper.

In Fig. S.10, we display the actually calculated data points. From these points, we obtain the contour plots of Fig. 3 in the main text. For the $t' = t'' = 0$ case, we linearly interpolated some irrelevant (i.e., $\lambda \leq 0.6$) points: $(U/t, n) = (4.75, 0.775), (5.25, 0.775), (5.5, 0.75), (5.5, 0.775), (5.5, 0.8675)$ before making the contour plot.

As for the T_c calculation, we calculate the superconducting λ down to $T = t/100$, and extrapolated the λ vs. T curve (using the form $\lambda \approx a - b \ln(T)$) as in previous publications [5, 20]. As examples, we show in Fig. S.11 DGA results, fit function, and T_c for (a) $U = 7.5t, t' = -0.22t, t'' = 0.14t$ and (b) $U = 6t, t' = -0.24t, t'' = 0.16t$ results (corresponding the RbSr₂PdO₃ and $A'_2\text{PdO}_2\text{Cl}_2$, respectively).

Besides the superconducting eigenvalue, we also calculate the antiferromagnetic (AFM) susceptibility $\chi_{\text{sp}}(Q_{\text{max}}, \omega = 0)$. DGA respects constraints of the two-dimensionality (i.e., Mermin-Wagner theorem [23, 24]) and does not exhibit an antiferromagnetically ordered phase at finite temperatures (χ_{sp} remains finite). On the other hand, we can naturally expect that AFM will stabilize for a strongly fluctuating regime (dark red region in Fig. 3 of the main text) once allowing for a weak three-dimensionality, that are present in the actual materials.

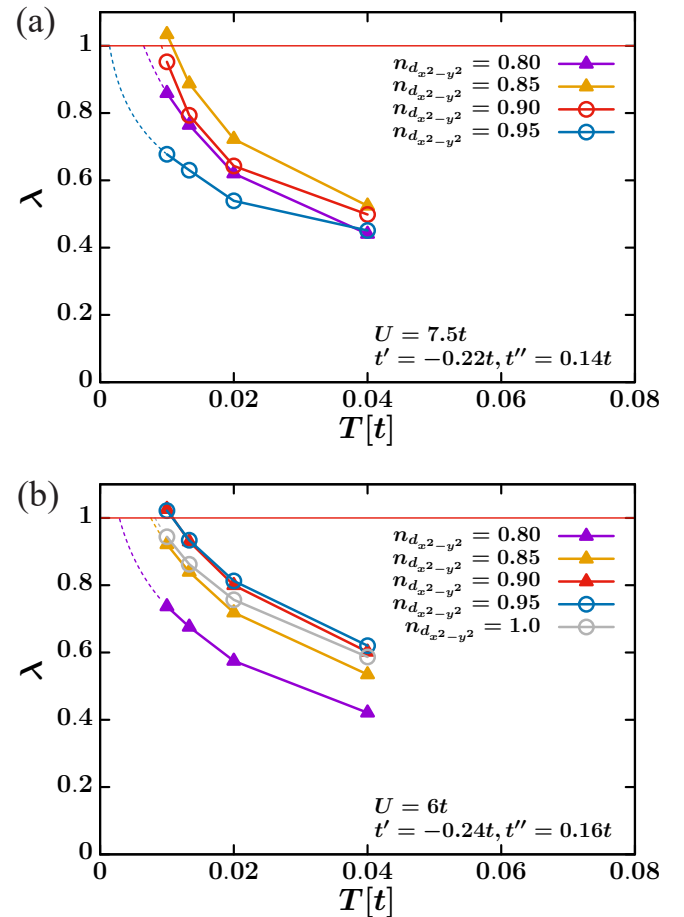


FIG. S.11. Temperature dependence of the superconductivity eigenvalue λ for (a) $U = 7.5t, t' = -0.22t, t'' = 0.14t$ and (b) $U = 6t, t' = -0.24t, t'' = 0.16t$. The extrapolation to $\lambda = 1$ yields T_c .

Lett. **77**, 3865 (1996).

- [3] M. Hirayama, T. Tadano, Y. Nomura, and R. Arita, Phys. Rev. B **101**, 075107 (2020).
- [4] K. Lee, B. Y. Wang, M. Osada, B. H. Goodge, T. C. Wang, Y. Lee, S. Harvey, W. J. Kim, Y. Yu, C. Murthy, S. Raghu, L. F. Kourkoutis, and H. Y. Hwang, arXiv:2203.02580 (2022).
- [5] M. Kitatani, L. Si, O. Janson, R. Arita, Z. Zhong, and K. Held, npj Quantum Materials **5**, 59 (2020).
- [6] L. Bellaiche and D. Vanderbilt, Phys. Rev. B **61**, 7877 (2000).
- [7] F. Tran and P. Blaha, Phys. Rev. Lett. **102**, 226401 (2009).
- [8] G. H. Wannier, Phys. Rev. **52**, 191 (1937).
- [9] N. Marzari and D. Vanderbilt, Phys. Rev. B **56**, 12847 (1997).
- [10] I. Souza, N. Marzari, and D. Vanderbilt, Phys. Rev. B **65**, 035109 (2001).
- [11] N. Marzari, A. A. Mostofi, J. R. Yates, I. Souza, and D. Vanderbilt, Rev. Mod. Phys. **84**, 1419 (2012).
- [12] A. A. Mostofi, J. R. Yates, Y.-S. Lee, I. Souza, D. Vanderbilt, and N. Marzari, Computer physics communications **178**, 685 (2008).

- [1] J. P. Perdew, A. Ruzsinszky, G. I. Csonka, O. A. Vydrov, G. E. Scuseria, L. A. Constantin, X. Zhou, and K. Burke, Phys. Rev. Lett. **100**, 136406 (2008).
- [2] J. P. Perdew, K. Burke, and M. Ernzerhof, Phys. Rev.

- [13] J. Kuneš, R. Arita, P. Wissgott, A. Toschi, H. Ikeda, and K. Held, *Computer Physics Communications* **181**, 1888 (2010).
- [14] V. I. Anisimov, I. V. Solovyev, M. A. Korotin, M. T. Czyzyk, and G. A. Sawatzky, *Phys. Rev. B* **48**, 16929 (1993).
- [15] M. Wallerberger, A. Haasöel, P. Gunacker, A. Kowalski, N. Parragh, F. Goth, K. Held, and G. Sangiovanni, *Computer Physics Communications* **235**, 388 (2019).
- [16] E. Gull, A. J. Millis, A. I. Lichtenstein, A. N. Rubtsov, M. Troyer, and P. Werner, *Rev. Mod. Phys.* **83**, 349 (2011).
- [17] J. Kaufmann and K. Held, [arXiv:2105.11211](https://arxiv.org/abs/2105.11211) (2021).
- [18] J. E. Gubernatis, M. Jarrell, R. N. Silver, and D. S. Sivia, *Phys. Rev. B* **44**, 6011 (1991).
- [19] A. W. Sandvik, *Phys. Rev. B* **57**, 10287 (1998).
- [20] M. Kitatani, R. Arita, T. Schäfer, and K. Held, *Journal of Physics: Materials* **5**, 034005 (2022).
- [21] M. Kitatani, T. Schäfer, H. Aoki, and K. Held, *Phys. Rev. B* **99**, 041115 (2019).
- [22] T. Schäfer, A. A. Katanin, M. Kitatani, A. Toschi, and K. Held, *Phys. Rev. Lett.* **122**, 227201 (2019).
- [23] P. C. Hohenberg, *Phys. Rev.* **158**, 383 (1967).
- [24] N. D. Mermin and H. Wagner, *Phys. Rev. Lett.* **17**, 1133 (1966).